A Supramolecular "Double-Cable" Structure with a 129_{44} Helix in a Columnar Porphyrin-C_{60} Dyad and its Application in Polymer Solar Cells

Chien-Lung Wang, Wen-Bin Zhang, Hao-Jan Sun, Ryan M. Van Horn, Rahul R. Kulkarni, Chi-Chun Tsai, Chain-Shu Hsu, Bernard Lotz, Xiong Gong, and Stephen Z. D. Cheng**

A novel porphyrin-C_{60} dyad (PCD1) is designed and synthesized to investigate and manipulate the supramolecular structure where geometrically isotropic [such as [60]fullerene (C_{60})] and anisotropic [such as porphyrin (Por)] units coexist. It is observed that PCD1 possesses an enantiomeric phase behavior. The melting temperature of the stable PCD1 thermotropic phase is 160 °C with a latent heat (ΔH) of 18.5 kJ mol^{-1}. The phase formation is majorly driven by the cooperative intermolecular Por–Por and C_{60}–C_{60} interactions. Structural analysis reveals that this stable phase possesses a supramolecular "double-cable" structure with one *p*-type Por core columnar channel and three helical *n*-type C_{60} peripheral channels. These "double-cable" columns further pack into a hexagonal lattice with $a = b = 4.65$ nm, $c = 41.3$ nm, $\alpha = \beta = 90°$, and $\gamma = 120°$. The column repeat unit is determined to possess a 129_{44} helix. With both donor (D; Pro) and acceptor (A; C_{60}) units having their own connecting channels as well as the large D/A interface within the supramolecular "double-cable" structure, PCD1 has photogenerated carriers with longer lifetimes compared to the conventional electron acceptor [6,6]-phenyl-C_{61}-butyric acid methyl ester. A phase-separated columnar morphology is observed in a bulk-heterojunction (BHJ) material made by the physical blend of a low band-gap conjugated polymer, [poly[2,6-(4,4-bis-(2-ethylhexyl)-4*H*-cyclopenta [2,1-b;3,4-b′]-dithiophene)-*alt*-4,7-(2,1,3-benzothiadiazole)] (PCPDTBT), and PCD1. With a specific phase structure in the solid state and in the blend, PCD1 is shown to be a promising candidate as a new electron acceptor in high performance BHJ polymer solar cells.

1. Introduction

In the cause of materials development, it is often necessary to exert control not only on the chemical structures at the molecular level, but also over the hierarchical physical structures across multiple length scales so that the functions at the molecular level can be eventually transferred and amplified to exhibit a desired macroscopic property. Building up such hierarchical structures requires understanding of various thermodynamic free energy pathways in addition to the kinetics of structure formation; such structures are critically important for the molecular design, chemical synthesis, and property control of new materials.

The emerging field of "plastic electronics" and its rapid development has been largely attributed to the investigation of π-conjugated molecules, due to their tunable optical and electronic properties and the potential of low-cost fabrications.[1–3] "Supramolecular electronics" has been conceptually proposed and recognized as an important approach to manipulate their properties through self-assembly.[4–15] The key feature of "supramolecular electronics" is to generate specific supramolecularly ordered structures based on the requirements of device configurations. For example, in organic solar cells, it is highly desired to have a phase-separated bicontinuous network morphology with a large donor (D)/acceptor (A) interface and separate channels for electron- and hole-transportation (ambipolar transport).[16–20] The term "double-cable" was originally coined to describe polymers which are composed of a *p*-type conjugated polymer donor backbone tethered by *n*-type acceptor moieties, such as [60]fullerene (C_{60}).[21–26] However, the lack of precise control over the secondary and further hierarchical physical structures of the polymers has not led to the anticipated device performance.

Recently, we have designed and investigated a supramolecular "double-cable" structure formed by a porphyrin-C_{60} dyad (PCD1 in **Scheme 1**) without the bulky 3,5-bis(dodecyloxy)benzyloxycarbonyl group on its C_{60} segment.[27] This less-hindered

C.-L. Wang, W.-B. Zhang, H.-J. Sun, R. M. Van Horn, R. R. Kulkarni, C.-C. Tsai, Prof. X. Gong, Prof. S. Z. D. Cheng
College of Polymer Science and Polymer Engineering
The University of Akron
Akron, Ohio 44325, USA
E-mail: xgong@uakron.edu; scheng@uakron.edu
Prof. C.-L. Wang, Prof. C.-H. Hsu
Department of Applied Chemistry
National Chiao Tung University
Hsinchu, Taiwan 30010, ROC
Prof. B. Lotz
Institut Charles Sadron
23, Rue du Loess
Strasbourg 67034, France

DOI: 10.1002/aenm.201200060

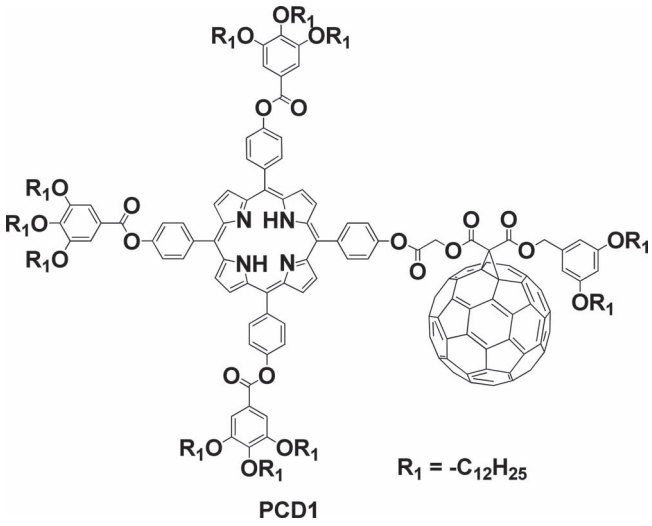

Scheme 1. Chemical structure of PCD1.

structure allows the C_{60} segments to interact with each other in forming parallel C_{60} inter-column channels with stacked porphyrin columns. Furthermore, a *trans*-di-C_{60}-substituted Zn(II) porphryin derivative also demonstrated a supramolecular structure with an alternating arrangement of donors and acceptors in a triclinic unit cell.[28,29]

In this article, we report the design, synthesis, structural characterization, and electronic properties of a novel porphyrin-C_{60} dyad. It is our purpose to construct the C_{60} channels within a porphyrin column (instead of the inter-C_{60} column channels as previously designed). This is because C_{60} now possesses the bulky 3,5-bis(dodecyloxy)benzyloxycarbonyl group to prevent interactions among the C_{60}s in the neighbouring columns. We have demonstrated that PCD1 contains *p*-type columnar channels, which are formed through the π–π stacking of porphyrin discotic liquid crystals (LCs) with the C_{60} pendants, which assemble into continuous *n*-type channels near the periphery of each column in a 129_{44} helix. These columns then packed into a hexagonal columnar LC phase at room temperature. To the best of our knowledge, this is the longest well-defined helical unit cell ever determined and reported for supramolecular structures.

Most studies of π-conjugated molecules are focused on the photo- and electro-properties in solution;[30–35] however, the highlight of this article is the study of the physical structure and phase behaviour in the bulk. This is also different from the supramolecular complexes of porphyrin and pristine C_{60} formed in solution, in which the type of solvents often played an essential role.[36–41] We have demonstrated that PCD1 shows promising results for optoelectronic applications, as a proof-of-concept design, exhibited by the long-lived charge carriers observed from time-resolved photoinduced absorption (PIA) spectra, the phase-separated morphology observed from the [poly[2,6-(4,4-bis-(2-ethylhexyl)-4*H*-cyclopenta[2,1-b;3,4-b′]-dithiophene)-*alt*-4,7-(2,1,3-benzothia-diazole)] (PCPDTBT):PCD1 blend thin films, and higher J_{sc} observed from the bulk heterojunction (BHJ) polymer solar cells. This is attributed to the designed supramolecular "double-cable" structure, and provides potential for further material optimization through chemical synthesis and structure perfection.

2. Results and Discussion

2.1. Synthesis of PCD1

The molecular design is based on porphyrin discotic LCs with pendant, covalently linked C_{60}s. The rationale for the particular interest of this design is twofold: first, the combination of porphyrin as an electron D and C_{60} as an electron A is known to exhibit a highly efficient, long-lived charge separation state;[31–35] and second, the discotic LC phase formation ensures the processibility and self-healing properties.[14] The formation of an ordered structure from the apparently incommensurate columnar-forming 2D porphyrin (Por) plane and isotropically aggregating 3D sphere C_{60}[42] is intriguing and requires a delicate balance among the C_{60}–C_{60}, Por–Por and C_{60}–Por interactions. The peripheral alkyl tails on C_{60} are designed as a layer of chemical shield to prevent intercolumnar C_{60}–C_{60} interactions, allowing only intracolumnar C_{60}–C_{60} interactions. At the smaller length scale, a supramolecular "double-cable" structure with separated D and A channels is anticipated in the supramolecular assemblies of PCD1. At larger length scales, these channels have to be cooperatively aligned into a phase structure to ensure the macroscopic electron and hole transports.

The synthesis of PCD1 was accomplished by two sequential Steglich esterfications in a straightforward way from 5,10,15,20-tetra-(*p*-hydroxyphenyl) porphyrin (**Scheme 2**) in good yield (around 70%). The products have been fully characterized by ^{1}H NMR, ^{13}C NMR, FT-IR, and MALDI-TOF spectrometry. The successful attachment of C_{60} was evidenced by

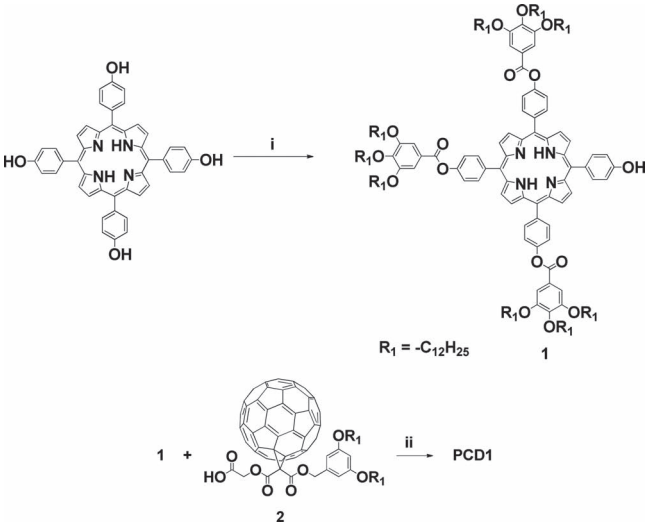

Scheme 2. Synthetic route of PCD1. Reagents and conditions: i) 3,4,5-tris-dodecyl-oxy benzoic acid, *N*,*N*′-diisopropylcarbodiimide (DIPC), 4-(dimethylamino) pyridinium toluene-*p*-sulfonate (DPTS), THF/CH_2Cl_2 = 1/2, 25 °C; and, ii) DIPC, DPTS, CH_2Cl_2, 25 °C.

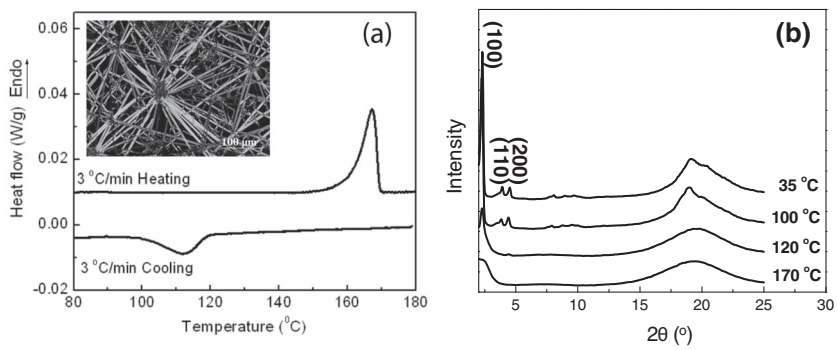

Figure 1. a) DSC thermograms of PCD1 at a scan rate of 3 °C min^{-1}; they show enantiotropic phase behavior. The inset is a POM micrograph of the ordered phase of PCD1. b) WAXD patterns of PCD1 at different temperatures during cooling at 3 °C min^{-1}.

the downfield shift of the chemical shifts for the protons on the phenyl ring of the phenol moiety from δ 8.09 and 7.21 ppm to δ 8.26 and 7.60 ppm in the ^{1}H NMR spectrum upon esterification (Figure S1 in the Supporting Information (SI)). The appearance of multiple chemical shifts between δ 135 to 145 ppm in the ^{13}C NMR spectrum of PCD1 (Figure S2, SI) could be assigned to the sp^2 carbons on C_{60}. The sharp absorption band at 527 cm^{-1} in the FT-IR spectrum of PCD1 (Figure S3, SI) was characteristic of the C_{60} core. The well-defined structures were further confirmed by the MALDI-TOF mass spectra (Figure S4, SI). There was only a single peak observed with an m/z value of 3968.33, which matches well with the calculated monoisotopic mass of PCD1 (3968.35 Da; SI, Figure S4b, inset). All the results clearly indicate the success of the reaction and confirm the chemical identity and purity of PCD1.

2.2. Phase Behaviors of PCD1

In thermogravimetric measurements, the 1% weight loss temperature is observed at 296 °C at a heating rate of 10 °C min^{-1} (Figure S5, SI), suggesting a high thermal stability of the compound. The phase behavior of PCD1 was then studied utilizing differential scanning calorimetry (DSC). The heating and subsequent cooling DSC thermal diagrams at a scan rate of 3 °C min^{-1} are shown in **Figure 1**a. Upon heating, a transition temperature of PCD1 appears at 160 °C with a latent heat (ΔH) of 18.5 kJ mol^{-1}. Above 160 °C, PCD1 enters the isotropic phase (I) as confirmed by the amorphous halos in the one-dimensional (1D) wide angle X-ray diffraction (WAXD) data (Figure 1b) and the complete darkness under cross polarizers in polarized optical microscopy (POM). Upon subsequent cooling, PCD1 exhibits an exothermic transition at 119 °C with an identical latent heat to that observed during heating. Thus, PCD1 possesses an enantiotropic phase behavior. The phase transition of a porphyrin derivative (Por1; **Table 1**), which has identical chemical structure to the porphyrin core and the peripheral alkyl tails, but no C_{60} unit, occurs at 149 °C with a latent heat of 14 kJ mol^{-1} (Table 1).[43] The transition entropies (ΔS) of Por1 and PCD1 are thus 33.2 and 42.7 (J mol^{-1} K^{-1}), respectively, calculated via the equilibrium transition temperatures and the ΔHs. Since the dodecyl tails are in their I state at these high temperatures, the ΔH and ΔS differences between Por1 and PCD1 must be largely attributed to the intermolecular C_{60} interactions in this ordered phase. The contribution of Por–C_{60} interactions in the ordered phase is limited, since the structural determination (vide infra) indicates that C_{60}s and Pors form separated nanodomains in the ordered structure. Therefore, the DSC results show that the phase formation is driven by both Por–Por and C_{60}–C_{60} interactions. Furthermore, since the latent heat is mainly attributed to porphyrins, the molecular design of PCD1 allows Por–Por interactions to dominate the formation of this ordered columnar phase.

2.3. Phase Structure Determinations of PCD1

The structure change was followed by 1D WAXD at different temperatures during cooling at 3 °C min^{-1}, as shown in Figure 1b. At 170 °C, only two diffuse halos are observed. The diffuse halo in the high 2θ angle region represents a short-range order at the segmental level within molecules, while another halo in the low 2θ angle region is attributed to the short-range order of whole molecules. With decreasing temperature to below 119 °C, sharp diffractions appear. The three diffractions are found to possess ratios of the scattering vector, q, of 1:$\sqrt{3}$:2 with corresponding d-spacings of 4.06, 2.34, and 2.03 nm, respectively, which can be indexed as the (100), (110), and (200) of a hexagonal lattice with $a = b = 4.65$ nm, $\alpha = \beta = 90°$, and $\gamma = 120°$. This hexagonal symmetry can be further verified via oriented samples using electron diffraction (ED) experiments in transmission electron microscopy (TEM). **Figures 2** and b show that the (hk0) diffractions are located along the equator, indicating that the columns and the c-axis are aligned along the meridian. The observation of the (110) diffraction without sample tilt (Figure 2a) and the (100) diffraction at a 30° tilt (Figure 2b) confirms the hexagonal symmetry. The corresponding POM image for the hexagonal phase is shown in the inset of Figure 1a.

Table 1. Summary of the transition temperatures (T_m), latent heats (ΔH), and transition entropies (ΔS) of Por1 and PCD1.

	Por1	PCD1
Chemical structure	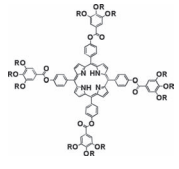	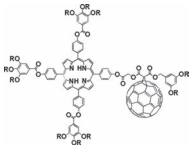
	R = -$C_{12}H_{25}$	R = -$C_{12}H_{25}$
T_m (°C)	149	160
ΔH (kJ mol^{-1})	14.0	18.5
ΔS (J mol^{-1} K^{-1})	33.2	42.7

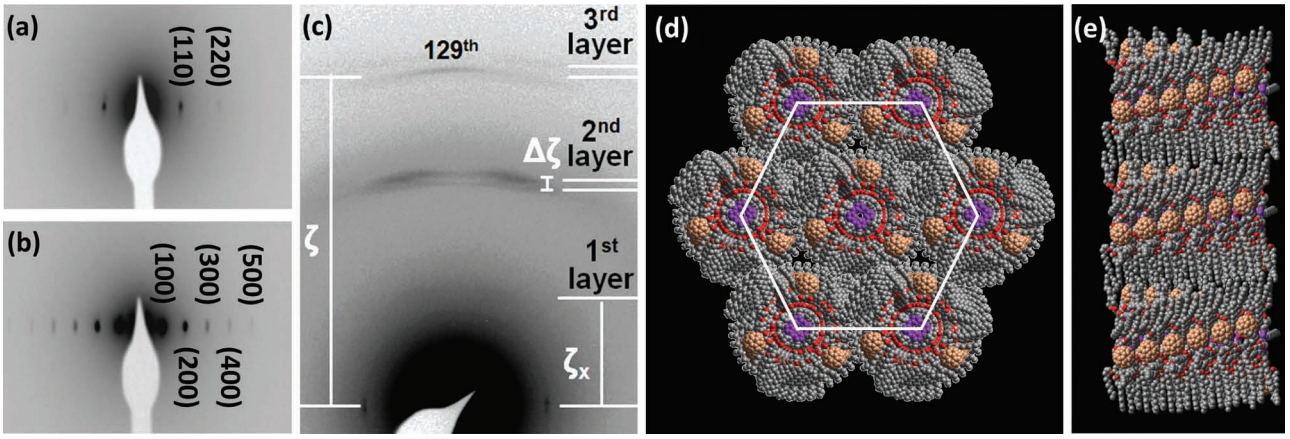

Figure 2. ED patterns of the Col_h phase of PCD1 at tilting angles a) 0°, and, b) 30° (tilt axis is along the meridian). c) ED patterns of the Col_h phase of PCD1 with contrast enhancement of the arcs on the meridian and quadrant. d) Top, and, e) side views of an energy-minimized model of the Col_h of PCD1. The model is built based on molecular mechanics simulation and experimental diffraction data (purple – porphyrin; brown – C_{60}).

The *c*-axis dimension of this unit cell is determined based on the ED pattern shown in Figure 2c where this axis is aligned along the meridian. The ED arcs along the meridian direction can be divided into three layers separated with reciprocal spacing, ζ_x, and with the meridian diffraction arc on the third layer. This feature signifies a structure close to a 3_1 helix. The translational vector (*p*) of the helix, which describes how far the repeating unit translates along the *c*-axis in each step, is determined to be 0.32 nm. Surprisingly, by precise calculation from the distance between the fine splitting in each layer line ($\Delta\zeta$) and the reciprocal spacing (ζ) of the diffractions at the meridian line, the structure was determined to be a 129_{44} helix (see the SI for details).[44,45] Thus, the meridian line represented actually the 129th layer line in reciprocal space and a full helical turn in real space contains a stack of 129 molecules rotated for 44 turns. In each helical step along the *c*-axis, the repeating unit translates 0.32 nm, and rotates $(44 \times 360°)/129 = 123°$. The *c* parameter is thus $129 \times 0.32 = 41.3$ (nm). The theoretical density with 129 molecules of PCD1 per unit cell is calculated to be 1.10 g cm^{-3}, which is in good agreement with the measured density of 1.09 g cm^{-3}. To the best of our knowledge, the formation of such a long period in a helical unit cell is rare, if not unprecedented, in self-assembled supramolecular structures. It should be noted that since PCD1 does not have a chiral center to guide the helical formation, the helical sense of the column could be either left-handed or right-handed, depending on the initial PCD1 stacking nucleus scheme. Nevertheless, the ED patterns suggest the existence of a long-range ordered helical structure with a defined sense for each column, meaning that once the helical sense is formed at the initial nucleus, it will be kept along the column. Moreover, these helical columns further packed into a hexagonal lattice irrespective of the helical senses. This is a typical hierarchical structure.

The detailed molecular packing of PCD1 was illustrated by computer simulation via the Accelrys Cerius[2] package using the universal force field. The 129_{44} helix can be constructed by stacking the porphyrin moieties of the PCD1 molecules along the *c*-axis to form the core channel of a column with C_{60} moieties packing near the periphery to form three separate, slightly twisted helical channels. These columns further pack into a hexagonal lattice. Figures 2d and e are the top and side views of the energy-minimized model of the helical columnar packing in the Col_h phase. **Figure 3**a

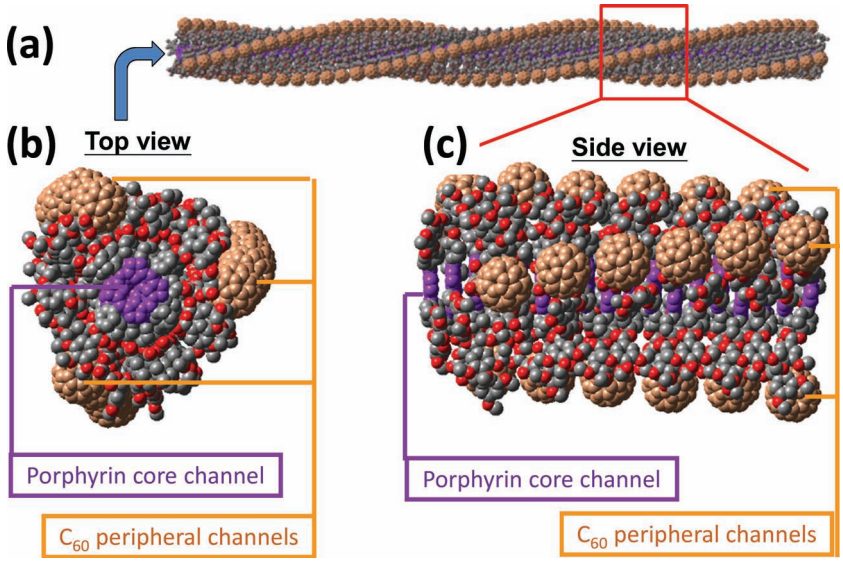

Figure 3. a) Illustration of the supramolecular "double-cable" helical structure of PCD1 and the porphyrin core channel and C_{60} peripheral channels in the 129_{44} helical structure. b) Enlarged top view, and, c) enlarged side view of an energy-minimized model of a stack of eighteen molecules of PCD1 based on molecular mechanics simulation and the experimental diffraction data (purple – porphyrin core; brown – C_{60}). Alkyl tails are omitted for clarity.

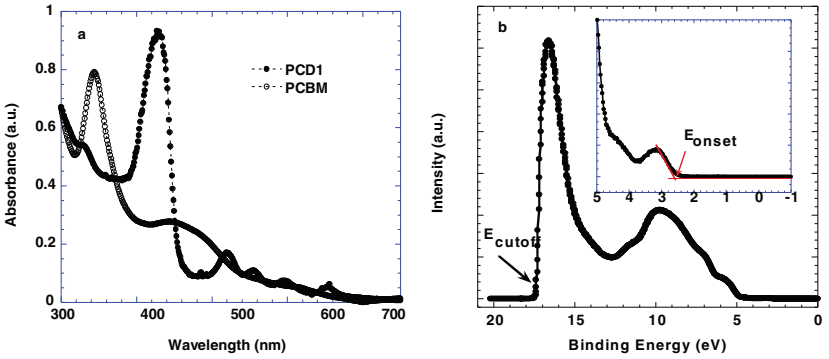

Figure 4. a) Absorption spectra of pristine thin films of PCD1 and PCBM, and, b) UPS spectrum of PCD1 at the secondary edge region. Inset is the HOMO region of PCD1.

demonstrates a single 129_{44} helical double-cable structure of PCD1s with the alkyl tails omitted for clarity. Figures 3b and c are the enlarged top and side views of the 129_{44} helix. The porphyrin core channel and the C_{60} peripheral channels can be clearly identified in the helical structure. Thus, this is a well-defined supramolecular "double-cable" structure since the D (porpyrin) and A (C_{60}) form individual continuous but separate channels. The formation of 129_{44} helix instead of the simple 3_1 helix can be rationalized by the fact that close packing of C_{60} requires a center-to-center distance of 1 nm,[42] which is larger than the spacing of three consecutive stacks ($3p$ = 0.96 nm). As a result, PCD1s have to rotate 368° in three consecutive translation steps along the *c*-axis so that the extra 8° of rotation creates a 0.28 nm offset on the radiant to accommodate the neighbouring C_{60}s (Figure S6b).

2.4. Optical and Electronic Properties of PCD1

UV-vis absorption spectra of PCD1 (**Figure 4**a) show that PCD1 has extensive absorption of solar radiation compared to PCBM, indicating that PCD1 possesses a higher light-harvesting efficiency than [6,6]-phenyl-C_{61}-butyric acid methyl ester (PCBM) in polymer solar cells (PSCs). The E_{LUMO} of PCD1 was determined by ultraviolet photoelectron spectroscopy (UPS) and absorption spectra. Figure 4b and its inset show the high binding energy cutoff (E_{cutoff}) and the HOMO region (0–5 eV) of the PCD1 thin film. The abscissa is the binding energy relative to the Fermi energy (E_F) of Au, which is defined by the energy of the electron before excitation relative to the vacuum level. The HOMO energy is determined to be –6.31 ± 0.03 eV based on the following formula, $E_{HOMO} = h\nu - (E_{cutoff} - E_{onset})$, where the incident photon energy is $h\nu$ = 21.2 eV and E_{onset} is the onset of the PCD1 film relative to the E_F of Au.[46,47] The LUMO energies were calculated using the HOMO level and the optical gap (E_g) obtained in the UV-vis absorption spectra (Figure 4a). For PCD1, E_{LUMO} is thus 3.67 ± 0.03 eV.

In order to confirm specifically the difference between PCD1 and PCBM, time-resolved photoinduced absorption (PIA) spectra of pristine PCD1 and PCBM thin films was investigated. **Figure 5**a compares the dynamics of the time-resolved PIA of PCD1 and PCBM pumped at 400 nm and probed at 480 nm where PCBM has strong absorption and PCD1 has negligible absorption. A much longer decay lifetime in PCD1 compared to that in the PCBM indicates the photogeneration of long-lived charge carriers, which is consistent with efficient intermolecular charge transfer from porphyrin to fullerenes.[48–50] Figure 5b compares the dynamics of the time resolved PIA in thin films of pristine PCPDTBT and the composites, PCPDTBT:PCD1 probed at 4.6 µm and pumped at 800 nm where PCPDTBT has strong absorption[51] but PCD1 has negligible absorption. In this mid-IR spectral region, where the well-known polaron signatures of PCPDTBT are detected, a relatively fast decay is observed in PCPDTBT. A much longer polaron lifetime in PCPDTBT:PCD1 compared to that in the pristine PCPDTBT indicates the photogeneration of long-lived carriers, that is consistent with efficient charge transfer between PCPDTBT to PCD1.[48–50] These data are in good agreement with results obtained from typical polymer:PCBM BHJ materials where charge transfer between the semiconducting polymer donor and the fullerene acceptor increases the lifetime of photogenerated mobile charge carriers.

To evaluate the properties of supramolecular "double-cable" structure of PCD1 in opto-electronic applications, BHJ PSCs were fabricated utilizing PCPDTBT blended with PCD1 (at a material volume ratio of 1:1). The device structure is ITO/PEDOT:PSS/PCPDTBT:PCD1/Al. A TEM bright field image of the PCPDTBT:PCD1 blend thin film with a similar thickness to the active layer in the PSC shows the morphology of locally oriented PCD1 columnar domains with a diameter around 10–20 nm embedded in the polymer matrix (**Figure 6**a). The ED arcs obtained in the blend film as shown in Figure 6b can be indexed identically as those in the ED patterns shown in Figure 2a and c. All the diffractions shown in Figure 6b can be assigned to the (*hkl*) diffractions of the Col_h unit cell and the 129_{44} helical structure of PCD1. This result indicates that the PCD1 domains in the blend possess the same phase structure as the ordered structure formed in pure PCD1. Thus, the TEM results of the blend indicate that the supramolecular

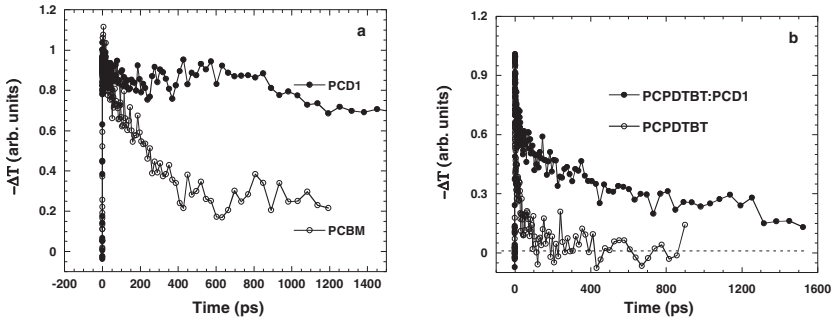

Figure 5. a) The decay dynamics of PCD1 and PCBM pumped at 400 nm and probed at 480 nm. b) Mid-IR transient decay dynamics of PCPDTBT:PCD1 and PCPDTBT pumped at 800 nm and probed at 4.6 µm.

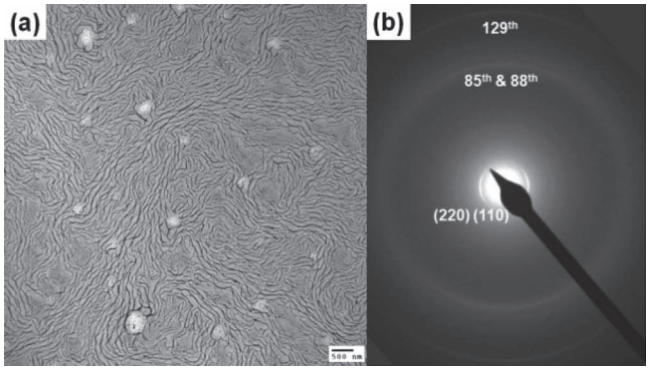

Figure 6. a) TEM image of the thin film of PCPDTBT/PCD1 blend (1.0:1.0). Locally oriented PCD1 columnar domains with a diameter around 10–20 nm are embedded in the polymer matrix. b) ED pattern of the Col_h phase domains of PCD1 embedded in the thin film of PCPDTBT/PCD1 blend observed in TEM.

"double-cable" structure is retained via the micro-phase separation from the PCPDTBT:PCD1 blend.

To evaluate the expected increase in both short-circuit current (J_{sc}) and open-circuit voltage (V_{oc}), PSCs were fabricated with PCPDTBT:PCD1. The charge separating layer was a PCPDTBT:PCD1 blend with 1:1 weight ratio. **Figure 7** shows the current density–voltage (J–V) characteristics of the PSCs with and without light illumination. Without light illumination, the PSCs show good diode performance with ratification larger than 10^3 at ±1 V. Under AM 1.5 G irradiation with 100 mW cm^{-2} intensity from calibrated solar simulator, the PSCs yield the power conversion efficiency (PCE) of 3.36%, with a J_{sc} of 13.5 mA cm^{-2}, a V_{oc} of 660 mV, and fill factor (FF) of 0.38. This result is better than those reported in literature using PCPDTBT:PCBM as an active layer,[51] despite its lower FF. The high V_{oc} can be rationalized as the high E_{LUMO} of PCD1

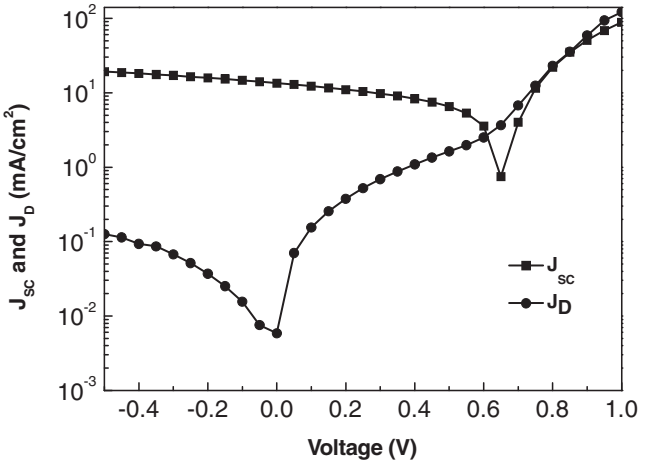

Figure 7. Current density–voltage (J–V) characteristics of the PCPDTBT:PCD1 PSCs under no light illumination and under the light source of AM 1.5 G irradiation with 100 mW cm^{-2} intensity from calibrated solar simulator.

obtained from UPS and absorption spectra.[52] More importantly, the large J_{sc} implies that the straight and reasonably interacted C_{60} channels in this supramolecular "double-cable" structure of PCD1 provides good charge transport properties. The results thus give rise to a potential improvement of the device performance via manipulating the supramolecular structure of π-conjugated molecules.

3. Conclusion

In summary, we have demonstrated an approach to manipulate the supramolecular "double-cable" structures formed via PCDs. By fine-tuning the intercolumnar C_{60}–C_{60} interactions via placing bulky groups on the C_{60} segment, liquid crystalline PCD1s have formed well-defined, thermally stable supramolecular "double-cable" helical structures with one *p*-type porphyrin core columnar channel and three helical *n*-type C_{60} peripheral channels. The helical structure of the column has been determined to be a 129_{44} helix. To the best of our knowledge, this represents the longest period for a well-defined helical repeating unit ever reported for supramolecular structures. The structure contains more or less parallel but separated arrays of hole and electron transport channels. The large D/A interface and separate, continuous charge transporting channels are desired for high photovoltaic performance. PCEs of 3.36% have been observed in the PSCs made with the blend of PCPDTBT:PCD1. This supramolecular approach allows further understanding of BHJ PSC structure-property relationships through molecular design and structural modification to optimize the electronic properties in these hierarchical structures.

4. Experimental Section

Synthesis: Details on the synthesis of **1** and **PCD1** are provided in the Supporting Information.

Thermal Property Characterization: The thermal transitions were identified with a Perkin-Elmer PYRIS DSC with an Intracooler 2P apparatus. The temperature and heat-flow scales were calibrated at heating and cooling rates of 5 °C min^{-1} using standard materials. Thermogravimetric measurements were conducted on a TA TGA Q500 instrument at 10 °C min^{-1} in a nitrogen atmosphere. Morphological observations on the micrometer scale were conducted using a POM (Olympus BH-2) coupled with a Mettler hot stage (FP-90).

Structural Characterization: 1D WAXD patterns were obtained with a Rigaku Multiflex 2 kW Automated Diffractometer using Cu K_α radiation (0.1542 nm). A hot stage was installed on the diffractometer to study phase structure transitions as a function of temperature. The peak positions were calibrated using silver behenate in the low-angle region ($2\theta < 15°$), and silicon crystals in the high-angle region ($2\theta > 15°$). Transmission electron microscopy (TEM) experiments were carried out with a Philips Tecnai 12 using an accelerating voltage of 120 kV. Selected area ED patterns were obtained using a TEM tilting stage to determine the crystal structure parameters. The *d*-spacings were calibrated using a TlCl standard. Basic unit cell parameters determined by crystallographic experimental data from WAXD and SAED experiments were used to build the crystallographic unit cell. Computer refinement was conducted to find the solutions with the least error between the calculated values and the experimental results. Computer molecular modelling was performed using the Cerius^2 package of Accelrys.

Time-Resolved Photoinduced Absorption: Films used for the time resolved PIA measurements were spin-cast onto sapphire substrates from

a 2 wt% dichlororbenzene solution, either pure PCD1 or PCBM, resulting in a film thickness of approximately 100 nm. The details of experimental set-up and the measurements are described in the literature.[48–50]

Bulk Heterojunction Polymer Solar Cells: Polymer solar cells were fabricated using PCPDTBT as the electron donor and PCD1 as the electron acceptor. The ITO-coated glass substrates were cleaned with detergent, distilled water, acetone, and isopropyl alcohol in an ultrasonic bath and then dried overnight in an oven at above 100 °C. After treatment of the ITO substrates with UV ozone for 40 min, highly conducting PEDOT:PSS was spin-cast from aqueous solution (thickness of approximately 40 nm). The substrates were dried at 160 °C for 10 min in air and transferred to a nitrogen-filled glovebox for spin-casting the PCPDTBT:PCD1 layer. Subsequently, a thin layer of cathode, Al (150 nm) was thermally deposited on BHJ layer through a shadow mask under vacuum. The area of the cathode that defines the active area of the device was 4.5 mm^2. All data were obtained under white light AM1.5G illumination from a calibrated solar simulator with irradiation intensity of 100 mW cm^{-2}.

Morphological Observation of PCPDTBT:PCD1 Blend: To obtain the morphology of the PCPDTBT:PCD1 blend, TEM samples were prepared by spin-casting a 2 wt% dichlororbenzene solution of PCPDTBT/PCD1 blend (1.0:1.0) resulting in a film thickness of approximately 100 nm on carbon-coated mica surfaces. The samples were then heated to 180 °C, cooled to 140 °C, and annealed at 140 °C for 12 h. After the annealing process, the samples were removed from the mica surface and collected on copper grids for TEM analysis.

Supporting Information

Supporting Information is available from the Wiley Online Library or from the author.

Acknowledgements

This work was supported by the National Science Foundation (DMR-0906898) and the Collaborative Center for Polymer Photonics, AFOSR. We appreciate Prof. Alan Heeger and his group at UC Santa Barbara for assistance with ultrafast spectrocopy measurements. We also thank Dr. Xiaopeng Li and Prof. Chrys Wesdemiotis for assistance with the MALDI-TOF mass spectra measurements.

Received: January 21, 2012
Revised: February 28, 2012
Published online: May 7, 2012

[1] A. J. Heeger, *Rev. Mod. Phys.* **2001**, *73*, 681.
[2] H. Shirakawa, *Rev. Mod. Phys.* **2001**, *73*, 713.
[3] A. G. MacDiarmid, *Rev. Mod. Phys.* **2001**, *73*, 701.
[4] J. M. Lehn, *Proc. Natl. Acad. Sci. USA* **2002**, *99*, 4763.
[5] D. Astruc, E. Boisselier, C. T. Ornelas, *Chem. Rev.* **2010**, *110*, 1857.
[6] J. M. Lehn, *Rep. Prog. Phys.* **2004**, *67*, 249.
[7] P. Leclère, M. Surin, P. Jonkheijm, O. Henze, A. P. H. J. Schenning, F. Biscarini, A. C. Grimsdale, W. J. Feast, E. W. Meijer, K. Müllen, J. L. Brédas, R. Lazzaroni, *Eur. Polym. J.* **2004**, *40*, 885.
[8] K. Tashiro, T. Aida, *Chem. Soc. Rev.* **2007**, *36*, 189.
[9] M. D. Watson, A. Fechtenkotter, K. Mullen, *Chem. Rev.* **2001**, *101*, 1267.
[10] M. O'Neill, S. M. Kelly, *Adv. Mater.* **2011**, *23*, 566.
[11] H. Liu, J. Xu, Y. Li, Y. Li, *Acc. Chem. Res.* **2010**, *43*, 1496.
[12] R. Li, W. Hu, Y. Liu, D. Zhu, *Acc. Chem. Res.* **2010**, *43*, 529.
[13] L. C. Palmer, S. I. Stupp, *Acc. Chem. Res.* **2008**, *41*, 1674.
[14] S. Laschat, A. Baro, N. Steinke, F. Giesselmann, C. Hägele, G. Scalia, R. Judele, E. Kapatsina, S. Sauer, A. Schreivogel, M. Tosoni, *Angew. Chem., Int. Ed.* **2007**, *46*, 4832.
[15] F. J. M. Hoeben, P. Jonkheijm, E. W. Meijer, A. P. H. J. Schenning, *Chem. Rev.* **2005**, *105*, 1491.
[16] J. L. Delgado, P.-A. Bouit, S. Filippone, M. A. Herranz, N. Martin, *Chem. Commun.* **2010**, *46*, 4853.
[17] W. Cai, X. Gong, Y. Cao, *Sol. Energy Mater. Sol. Cells* **2010**, *94*, 114.
[18] C. J. Brabec, S. Gowrisanker, J. J. M. Halls, D. Laird, S. Jia, S. P. Williams, *Adv. Mater.* **2010**, *22*, 3839.
[19] S. Günes, H. Neugebauer, N. S. Sariciftci, *Chem. Rev.* **2007**, *107*, 1324.
[20] B. Christoph, *J. Sol. Energy Mater. Sol. Cells***2004**, *83*, 273.
[21] M. Catellani, S. Luzzati, N.-O. Lupsac, R. Mendichi, R. Consonni, A. Famulari, S. V. Meille, F. Giacalone, J. L. Segura, N. Martin, *J. Mater. Chem.* **2004**, *14*, 67.
[22] A. Cravino, N. S. Sariciftci, *J. Mater. Chem.* **2002**, *12*, 1931.
[23] F. Zhang, M. Svensson, M. R. Andersson, M. Maggini, S. Bucella, E. Menna, O. Inganäs, *Adv. Mater.* **2001**, *13*, 1871.
[24] A. M. Ramos, M. T. Rispens, J. K. J. van Duren, J. C. Hummelen, R. A. J. Janssen, *J. Am. Chem. Soc.* **2001**, *123*, 6714.
[25] A. Cravino, G. Zerza, M. Maggini, S. Bucella, M. Svensson, M. R. Andersson, H. Neugebauer, N. S. Sariciftci, *Chem. Commun.* **2000**, 2487.
[26] T. Benincori, E. Brenna, F. Sannicolò, L. Trimarco, G. Zotti, P. Sozzani, *Angew. Chem.* **1996**, *108*, 718.
[27] C.-L. Wang, W.-B. Zhang, R. M. Van Horn, Y. Tu, X. Gong, S. Z. D. Cheng, Y. Sun, M. Tong, J. Seo, B. B. Y. Hsu, A. J. Heeger, *Adv. Mater.* **2011**, *23*, 2951.
[28] V. Luchnikov, D. Anokhin, S. Z. D. Cheng, C.-L. Wang, G. Bar, D. A. Ivanov, *J. Appl. Crystallogr.* **2011**, *44*, 540.
[29] C.-L. Wang, W.-B. Zhang, C.-H. Hsu, H.-J. Sun, R. M. Van Horn, Y. Tu, D. V. Anokhin, D. A. Ivanov, S. Z. D. Cheng, *Soft Matter* **2011**, *7*, 6135.
[30] S. Handa, F. Giacalone, S. A. Haque, E. Palomares, N. Martín, J. R. Durrant, *Chem. Eur. J.* **2005**, *11*, 7440.
[31] G. de Miguel, M. Wielopolski, D. I. Schuster, M. A. Fazio, O. P. Lee, C. K. Haley, A. L. Ortiz, L. Echegoyen, T. Clark, D. M. Guldi, *J. Am. Chem. Soc.* **2011**, *133*, 13036.
[32] D. M. Guldi, C. Luo, M. Prato, A. Troisi, F. Zerbetto, M. Scheloske, E. Dietel, W. Bauer, A. Hirsch, *J. Am. Chem. Soc.* **2001**, *123*, 9166.
[33] C. Luo, D. M. Guldi, H. Imahori, K. Tamaki, Y. Sakata, *J. Am. Chem. Soc.* **2000**, *122*, 6535.
[34] H. Imahori, Y. Sakata, *Adv. Mater.* **1997**, *9*, 537.
[35] H. Imahori, K. Hagiwara, M. Aoki, T. Akiyama, S. Taniguchi, T. Okada, M. Shirakawa, Y. Sakata, *J. Am. Chem. Soc.* **1996**, *118*, 11771.
[36] T. Umeyama, N. Tezuka, F. Kawashima, S. Seki, Y. Matano, Y. Nakao, T. Shishido, M. Nishi, K. Hirao, H. Lehtivuori, N. V. Tkachenko, H. Lemmetyinen, H. Imahori, *Angew. Chem., Int. Ed.* **2011**, *50*, 4615.
[37] P. D. W. Boyd, C. A. Reed, *Acc. Chem. Res.* **2004**, *38*, 235.
[38] T. Yamaguchi, N. Ishii, K. Tashiro, T. Aida, *J. Am. Chem. Soc.* **2003**, *125*, 13934.
[39] V. Georgakilas, F. Pellarini, M. Prato, D. M. Guldi, M. Melle-Franco, F. Zerbetto, *Proc. Natl. Acad. Sci. USA* **2002**, *99*, 5075.
[40] M. M. Olmstead, D. A. Costa, K. Maitra, B. C. Noll, S. L. Phillips, P. M. Van Calcar, A. L. Balch, *J. Am. Chem. Soc.* **1999**, *121*, 7090.
[41] P. D. W. Boyd, M. C. Hodgson, C. E. F. Rickard, A. G. Oliver, L. Chaker, P. J. Brothers, R. D. Bolskar, F. S. Tham, C. A. Reed, *J. Am. Chem. Soc.* **1999**, *121*, 10487.
[42] P. A. Heiney, J. E. Fischer, A. R. McGhie, W. J. Romanow, A. M. Denenstein, J. P. McCauley Jr., A. B. Smith, D. E. Cox, *Phys. Rev. Lett.* **1991**, *66*, 2911.
[43] X. Zhou, S.-W. Kang, S. Kumar, R. R. Kulkarni, S. Z. D. Cheng, Q. Li, *Chem. Mater.* **2008**, *20*, 3551.

[44] B. Lotz, J. C. Wittmann, *Materials Science and Technology*, Vol. *12* (Eds: R. W. Cahn, P. Haasen, E. J. Kramer), Wiley-VCH, Weinheim, Germany **1993**.
[45] F. Auriemma, C. De Rosa, *Macromolecules* **2009**, *42*, 5179.
[46] J. H. Seo, T.-Q. Nguyen, *J. Am. Chem. Soc.* **2008**, *130*, 10042.
[47] W. R. Salaneck, M. Lögdlund, M. Fahlman, G. Greczynski, T. Kugler, *Mater. Sci. Eng., R* **2001**, *34*, 121.
[48] M. Tong, N. E. Coates, D. Moses, A. J. Heeger, S. Beaupré, M. Leclerc, *Phys. Rev. B* **2010**, *81*, 125210.
[49] C. X. Sheng, M. Tong, S. Singh, Z. V. Vardeny, *Phys. Rev. B* **2007**, *75*, 085206.
[50] M. Tong, S. Cho, J. T. Rogers, K. Schmidt, B. B. Y. Hsu, D. Moses, R. C. Coffin, E. J. Kramer, G. C. Bazan, A. J. Heeger, *Adv. Funct. Mater.* **2010**, *20*, 3959.
[51] D. Mühlbacher, M. Scharber, M. Morana, Z. Zhu, D. Waller, R. Gaudiana, C. Brabec, *Adv. Mater.* **2006**, *18*, 2884.
[52] M. C. Scharber, D. Mühlbacher, M. Koppe, P. Denk, C. Waldauf, A. J. Heeger, C. J. Brabec, *Adv. Mat.* **2006**, *18*, 789.